

Stress Analysis on Triangular-Aperture Geogrid-Reinforced Bases over Weak Subgrade Under Cyclic Loading

An Experimental Study

Yu Qian, Jie Han, Sanat Kumar Pokharel, and Robert L. Parsons

Geogrids have been successfully used to improve soft subgrade and reinforce weak base courses for low-volume roads by providing lateral confinement. However, uniaxial and biaxial geogrids with rectangular or square apertures cannot provide uniform resistance in all directions. A new geogrid product with triangular apertures was developed and introduced into the market to overcome this problem. The triangular-aperture geogrid has a more stable grid structure and can provide uniform resistance in all directions compared with uniaxial and biaxial geogrids. However, the performance of triangular-aperture geogrid-reinforced bases has not been well evaluated. In this study, unreinforced and triangular-aperture geogrid-reinforced bases over a weak subgrade were constructed in a large geotechnical testing box ($2 \times 2.2 \times 2$ m) at the University of Kansas and tested under cyclic loading. During the tests, surface deformations and vertical stresses at the interface between the base and the subgrade were monitored. The test results showed that triangular-aperture geogrids reduced permanent surface deformations and vertical stresses at the interface compared with an unreinforced base. The benefit became more pronounced when a heavier-duty geogrid was used. The backcalculations from the measured vertical stresses at the interface between base and subgrade showed that the stress distribution angle and the modulus ratio of base course to subgrade decreased with an increase in the number of cycles. The rates of reduction in the stress distribution angle and the modulus ratio for the unreinforced base were faster than those for the reinforced bases. This paper focuses on the stress analysis of the test sections under cyclic loading.

Geogrids, a major type of geosynthetics, are commonly uniaxial and biaxial, with rectangular or square apertures. They have been successfully used for soil reinforcement in slopes, walls, roads, and foundations. Biaxial geogrids are commonly used for subgrade improvement and base reinforcement in roadway applications, including low-volume roads. Laboratory and field test data have demonstrated the improved performance of geogrid-reinforced unpaved and paved

roads. Das and Shin (1) pointed out that the most effective location of the geosynthetic for subgrade improvement is at the interface between the selected granular material and the subgrade. In this location, the geosynthetic provides separation, lateral restraint of the overlying granular material, and a tensioned membrane effect when deformed extensively. Because of their apertures, geogrids can interlock with aggregates in the base course and form a confined zone if there is an appropriate relationship between the aperture size of the geogrid and the particle size of the aggregate (2, 3). The confinement due to the geogrid–aggregate interlocking can increase the modulus of the base course, which leads to the distribution of vertical stresses over a wider subgrade area and consequently a reduction of vertical deformation in the subgrade (4, 5). Design methods are available for biaxial geogrid–reinforced unpaved roads in, for example, Giroud and Han (4, 5).

It is obvious that uniaxial geogrids have tensile resistance only in one direction; however, they are rarely used in base courses for roadway applications. Different from uniaxial geogrids, biaxial geogrids are commonly used at the interface between base course and subgrade or within the base course for roadway applications. As Dong et al. (6) demonstrated, biaxial geogrids cannot provide uniform tensile resistance when subjected to tension in different directions. Biaxial geogrids have higher tensile resistance in the machine and cross-machine directions but much lower resistance in other directions, especially in the 45° loading direction. Traffic loading can be channelized (e.g., highways) or random (e.g., construction sites and parking lots). Even in the channelized roads, the stresses applied to the geogrids can vary in the magnitude and direction due to stress rotation from the traffic loading. Therefore, the geogrids in the base course are always subjected to loading in different directions.

A new geogrid product with triangular apertures was developed and introduced into the market to overcome the nonuniform tensile-resistance problem of the biaxial geogrid for roadway applications. Because the triangular-aperture geogrid has a more stable grid structure than earlier designs, it can provide more uniform resistance in all directions compared with biaxial geogrids. Giroud (7) noted that the triangular structure of a geogrid presents many probable benefits over biaxial structures, including improved interlock, improved stress transfer from soil to geogrid, and improved distribution of stresses within the geogrid structure. Dong et al. (8) demonstrated from laboratory plate load tests that triangular-aperture geogrids are more efficient than biaxial geogrids in increasing ultimate bearing capacities of reinforced bases under static loading in relation to the ratio of bearing capacity to geogrid mass. The numerical results by Dong et al. (9) also

Y. Qian, Department of Civil and Environmental Engineering, University of Illinois at Urbana–Champaign, 3212 Newmark Civil Engineering Laboratory, 205 North Mathews, Urbana, IL 61801. J. Han, S. K. Pokharel, and R. L. Parsons, Department of Civil, Environmental, and Architectural Engineering, University of Kansas, 2150 Learned Hall, 1530 West 15th Street, Lawrence, KS 66045-7609. Corresponding author: J. Han, jiehan@ku.edu.

Transportation Research Record: Journal of the Transportation Research Board, No. 2204, Transportation Research Board of the National Academies, Washington, D.C., 2011, pp. 83–91.
DOI: 10.3141/2204-11

showed that triangular-aperture geogrids have more uniform distributions in tensile strength and stiffness than biaxial geogrids. However, because of the relatively recent introduction of this product, the performance of triangular-aperture geogrid-reinforced bases has not been well evaluated. Research is needed to evaluate the performance of this new type of geogrid. The objective of this study was to verify the performance of triangular-aperture geogrids for subgrade improvement and provide technical data that are useful for practice and future research.

This study investigated the performance of triangular-aperture geogrid-reinforced bases over a weak subgrade under cyclic loading. The research results are applicable to low-volume unpaved roads. Four laboratory cyclic plate load tests were conducted in a large test box to investigate the influence of triangular-aperture geogrids on the reduction in permanent deformations and vertical stresses at the interface between the base and the subgrade compared with an unreinforced base. This paper focuses on a stress analysis of the test results. Because of space limitations here, displacement analysis will be presented in a future publication.

TEST MATERIALS

Geogrid

Three triangular-aperture geogrids (a regular-duty grade, T1; a medium-duty grade, T2; and a heavy-duty grade, T3) made of polypropylene were used in this experimental study. One grade of triangular-aperture geogrid is shown in Figure 1. The index and mechanical properties of these three geogrids were provided by the manufacturer and are presented in Table 1. For the three geogrids, rib depth, aperture stability modulus, and radial stiffness increase from T1 to T2 to T3.

Base Material

AB-3 aggregate, well graded and commonly used in Kansas for low-volume roads, was adopted as the base material for this study. This material has the following physical properties: specific gravity (G_s) = 2.69, liquid limit (LL) = 20, plastic limit (PL) = 13, mean particle size

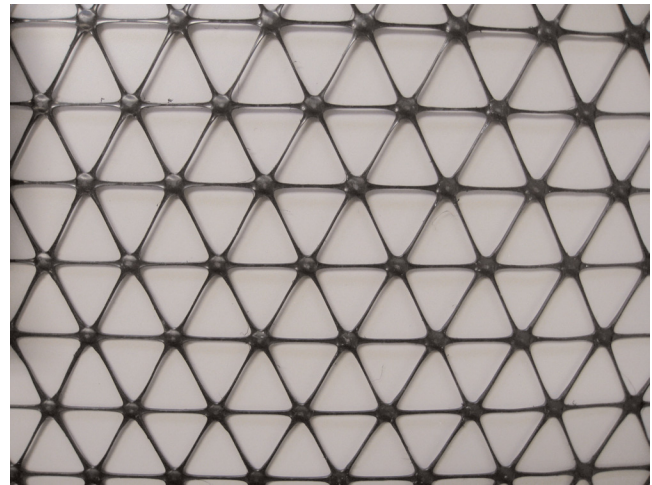


FIGURE 1 Triangular-aperture geogrid.

(d_{50}) = 7.0 mm, coefficient of curvature (C_c) = 2.25, and coefficient of uniformity (C_u) = 133. Standard Proctor compaction tests were performed to obtain the compaction curve for AB-3, as shown in Figure 2. The maximum dry density is 2.08 g/cm³, which corresponds to an optimum moisture content of 10.2%. A series of laboratory unsoaked California bearing ratio (CBR) tests (following ASTM D1188) for the base material were performed at different water contents. The curve of CBR versus moisture content is presented in Figure 2, which shows a decrease in the CBR value with an increase in the moisture content. As discussed later, the average CBR value of the base course over the subgrade in each box test was approximately 20% when the base course was compacted at a moisture content of 10.0%. This CBR value was estimated by the dynamic cone penetration (DCP) test after the preparation of the base course. The lower CBR value of the base material in the box test than that in the laboratory compaction mold resulted from less confinement of the base course in the large box test (4). For each layer of construction, the total mass of material placed was based on the calculated moist soil weight, and it was compacted to the volume marked on the test box wall to ensure that the desired density was achieved. The moisture content of

TABLE 1 Index and Mechanical Properties of Three Triangular-Aperture Geogrids

Index Property	Longitudinal			Diagonal			Transverse		
	T1	T2	T3	T1	T2	T3	T1	T2	T3
Rib pitch (mm)	40	40	40	40	40	40			
Midrib depth (mm)				1.2	1.6	2.0	1.2	1.4	1.6
Midrib width (mm)				1.1	1.0	1.0	1.1	1.2	1.3
Rib shape	Rectangular								
Aperture	Triangular								
Mechanical Properties	T1			T2			T3		
Junction efficiency (percentage)	93			93			93		
Aperture stability modulus (kg-cm/deg@5.0 kg-cm)	3.0			3.6			5.6		
Radial stiffness (kN/m @0.5% strain)	225			300			365		

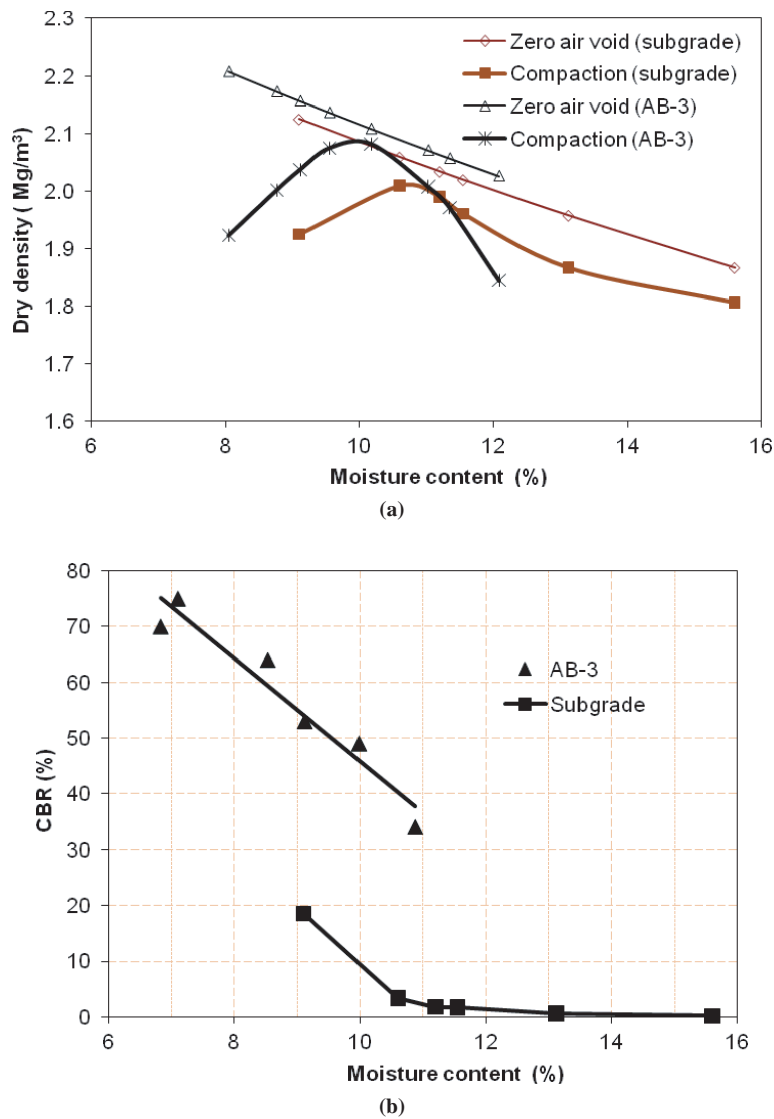


FIGURE 2 Compaction curves and CBR values of AB-3 aggregate and subgrade: (a) compaction curves and (b) CBR values.

the material was tested before and after mixing with water to ensure that the desired moisture content was reached within a difference of $\pm 0.1\%$. DCP tests were performed at a minimum of four locations in the base course and subgrade after compaction to verify their strengths.

Subgrade Material

The weak subgrade was an artificial soil composed of a mixture of 75% Kansas River sand and 25% kaolin by weight. The Kansas River sand used in this study was a poorly graded subrounded river sand having the following properties: $G_s = 2.62$, $d_{50} = 0.54$ mm, $C_c = 0.95$, and $C_u = 3.1$. The average particle size of the kaolin was 1.02 μm . Standard Proctor compaction tests were performed to obtain the compaction curve for the subgrade, as shown in Figure 2. The maximum dry density was 2.01 g/cm^3 , which corresponds to an optimum moisture content of 10.8%. A series of laboratory unsoaked CBR tests (ASTM D1188) for the subgrade were performed at different water contents. The curve of CBR versus moisture content is presented in

Figure 2. The subgrade soil was compacted at a water content of 11.4% for the box tests to achieve its CBR value at approximately 2.0%. The same procedure for the base compaction was adopted to control the moisture content and density of the subgrade during preparation. Vane shear tests were performed at a minimum of five locations for each lift of the subgrade after compaction to ensure that the desired subgrade strength was achieved. The subgrade strength was verified by DCP tests after each test section was constructed.

TEST SETUP

The test box available at the University of Kansas and used in this study is schematically shown in Figure 3, with one reinforced section as an example. The system used for the cyclic loading was an MTS hydraulic loading system. The steel loading plate had a diameter of 0.3 m and thickness of 0.018 m, with several stiffeners. Cyclic loading tests were conducted for both unreinforced and reinforced bases. The cyclic loading wave started with a 0.5-kN seating load, linearly

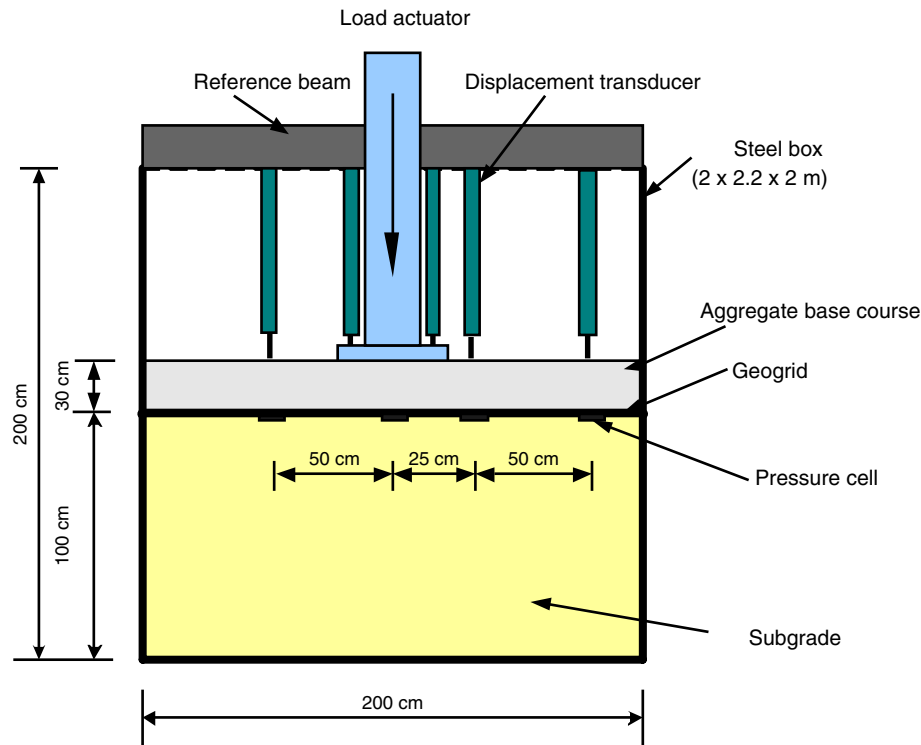


FIGURE 3 Setup of cyclic plate loading test.

increased to a peak load of 40 kN in 0.3 s, maintained for 0.2 s, linearly decreased to a trough load of 0.5 kN, and maintained for 0.5 s to complete one cycle of loading. The frequency of this wave was 0.77 Hz. The peak load was selected to simulate a single wheel load of 40 kN (equal to half an axle load of 80 kN and a tire contact pressure of 550 kPa).

The instrumentation and data acquisition system included four earth pressure cells and five displacement transducers. The earth pressure cells and displacement transducers were a strain gauge type, and they were made of stainless steel and had an outer diameter of 50 mm and thickness of 11.3 mm. The maximum capacity of these earth pressure cells was 500 kPa, which is higher than the expected maximum vertical stress at the interface between base and subgrade. The displacement transducers had two displacement ranges, 50 and 100 mm. Three larger-range displacement transducers were placed above and near the loading plate (i.e., 25 cm from the center of the plate). Two smaller range displacement transducers were placed at 50 and 75 cm from the center of the plate because smaller displacements at these two locations were expected. The larger and smaller range displacement transducers had sensitivities of 200 and 100 $\mu\text{e}/\text{mm}$ and frequency responses of 6 and 3 Hz, respectively.

In total, four tests were performed with the same base thickness of 0.3 m: one unreinforced section and three reinforced sections with three different triangular-aperture geogrids (i.e., T1, T2, and T3).

DISCUSSION OF RESULTS

Consistency of CBR Profiles

The test sections were designed to have a 20% CBR base course over a 2% CBR subgrade. Figure 4 shows the CBR profiles for these test

sections, which were estimated by means of the DCP tests on the basis of the following formula (10):

$$\text{CBR} = 292 / (\text{PI} \times 25.4)^{1.12} \quad (1)$$

where PI = penetration index (in. per blow), which is calculated on the basis of the penetration of each blow. The base materials within 5 cm above the top of the subgrade had lower CBR values because the subgrade was too weak to ensure proper compaction within this range. Figure 4 shows that the average CBR values for the base courses and the subgrade were approximately 20% and 2%, respectively. In general, the CBR values for all four test sections were consistent and comparable.

Repeatability of Test Results

The repeatability of test results was examined during this study. Details about this examination were provided in Qian (11) and are not repeated in this paper. Qian (11) showed that the test results based on the above-described procedures to prepare test sections and conduct cyclic testing had reasonable repeatability.

Permanent Deformation

A permanent deformation of the loading plate at 75 mm was used as the criterion to terminate a cyclic loading test. This criterion was used by Giroud and Han (4, 5) to define the failure of unpaved roads. Figure 5 presents the permanent deformations of the loading plate versus the number of loading cycles for the unreinforced and reinforced

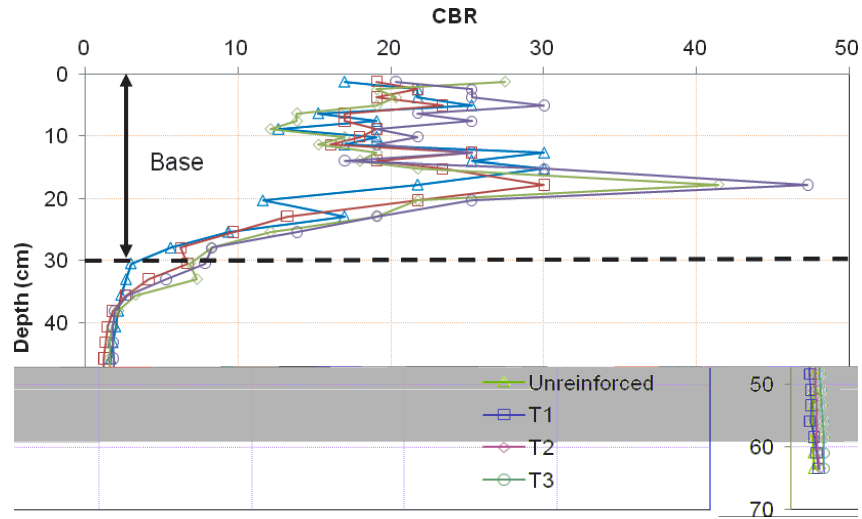


FIGURE 4 CBR profiles.

bases by T1, T2, and T3 geogrids, respectively. It is shown that the permanent deformations for all test sections increased with the number of cycles. The permanent deformations increased more slowly for the reinforced bases than for the unreinforced base. The heavy-duty geogrid, T3, was more effective in reducing the permanent deformation and the rate of deformation increase than the medium-duty geogrid, T2, the regular-duty geogrid, T1, and the unreinforced bases. It is also shown that the permanent deformations for all bases were similar at the initial few cycles because the geogrid was not mobilized. With an increase of the number of loading cycles, the benefit of geogrids became more obvious after the geogrid was mobilized.

To demonstrate the benefit of the geogrids, a traffic benefit ratio (TBR) or an improvement factor is defined here as the ratio of the number of cycles for the reinforced base to that for the unreinforced base at the same permanent deformation:

$$TBR = \frac{N_{reinforced}}{N_{unreinforced}} \quad (2)$$

where $N_{reinforced}$ is the number of cycles for the reinforced base at a certain permanent deformation and $N_{unreinforced}$ is the number of cycles for the unreinforced base at the same permanent deformation.

The calculated TBR values at 25-, 50-, and 75-mm permanent deformations are presented in Table 2. The table shows that the higher grade triangular-aperture geogrid had a larger TBR. Therefore, the T3 geogrid performed best of all three geogrids. The performance of the geogrids from the best to the least was T3, T2, and T1, which is the same order as the levels of robustness, unit weight, rib thickness, and mechanical properties of these geogrids, and as expected for this specific family of geogrid products. The TBRs for the T1 and T2 geogrids were almost constant at different permanent deformations; however, the TBRs for the T3 geogrid increased with permanent deformation. As discussed later, the increase in the vertical stress at the interface between the base and the subgrade and the decrease in the base-to-subgrade modulus ratio were much slower for the T3 geogrid-reinforced section than for those in other sections. These TBRs are experimental results and should not be used directly for design. A relationship should be established between the field and laboratory performances to apply these factors for design.

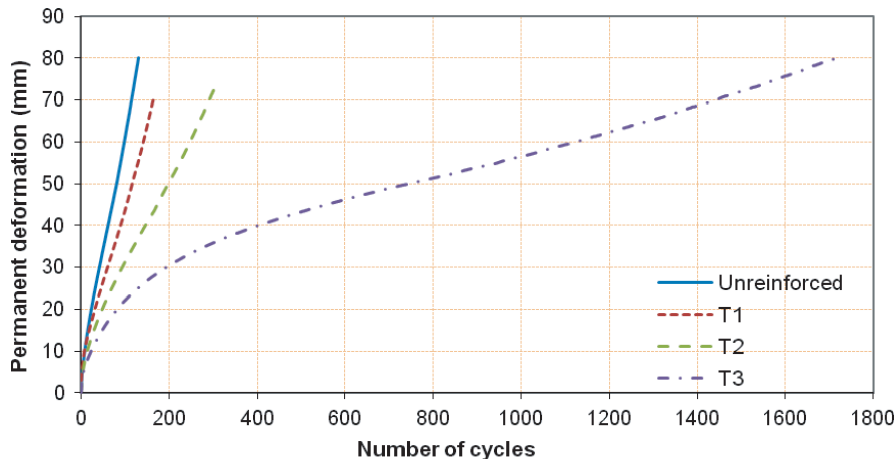


FIGURE 5 Permanent deformations of loading plate versus the number of cycles.

TABLE 2 Calculated Traffic Benefit Ratios

Deformation (mm)	T1 Geogrid	T2 Geogrid	T3 Geogrid
25	1.44	2.19	4.06
50	1.44	2.46	9.21
75	1.45	2.56	12.95
Average	1.44	2.40	8.74

Maximum Vertical Stress

For each test, vertical stresses at the interface between the base course and the subgrade were measured at four distances from the center: 0, 25, 50, and 75 cm. Figure 6 presents the measured maximum vertical stresses located along the center of the loading plate for all four test sections. The initial maximum vertical stresses, as shown in Figure 6, for all tests were close to each other because the geogrid was not mobilized at a small deformation. The maximum vertical stresses increased with the number of cycles, which is in good agreement with the finding by Gabr (12). The increase in the maximum vertical stress with the number of cycles was explained by Giroud and Han (4) as the reduction of the stress distribution angle due to deterioration of the base course. However, the maximum vertical stresses increased faster for the unreinforced base than for the reinforced bases. When the more-robust, thicker, and higher-mechanical-property geogrid was used, the maximum vertical stresses increased more slowly than when the less-robust, thinner, and lower-mechanical-property geogrid was used. The reason for this is that the more-robust, thicker, and higher-mechanical-property geogrid was more effective in maintaining the quality of the base course. The test results also show that the unreinforced base had the highest maximum vertical stress. The lower maximum vertical stresses in the reinforced bases are attributed to the benefit of the geogrids in reducing the rate of reduction in the stress distribution angles. The T3 geogrid-reinforced base had a larger stress distribution angle than the T2 geogrid-reinforced base, which had a larger distribution angle than the T1 geogrid-reinforced base. More discussion on the stress distribution is presented later.

Stress Distribution

Figure 7 presents the distributions of the measured vertical stresses at the interface between the base and the subgrade for the unreinforced and T1, T2, and T3 geogrid-reinforced base courses, respectively, at the 120th load cycle. The figure shows that the geogrids reduced the maximum vertical stresses at the center and transferred the vertical load to a wider area compared with the unreinforced base.

The test results show that the different grades of geogrids within the triangular-aperture geogrid family affected stress distribution. The more-robust, thicker, and higher-mechanical-property geogrids helped distribute the stresses more uniformly, thus reducing the maximum vertical stresses and resulting in less permanent deformation of the subgrade. Figure 7 shows that most vertical stresses were transferred to the area at the interface within two times the plate diameter.

Stress Distribution Angle

The stress distribution angle plays an essential role in stress distribution when a base course is over a weak subgrade and therefore requires further discussion. Three approaches exist to describe stress distribution and calculate the stress distribution angle: (a) based on the maximum vertical stress at the center of the interface between base and subgrade, (b) based on the area within which the majority of the load [Lawton (13) assumed 95%] is distributed, and (c) based on the shape of the deflections on the surface and at the interface between base and subgrade (14). Giroud and Han (4) adopted the first approach because the maximum vertical stress is more critical for bearing failure in fine-grained soils. The first approach was also adopted in this study.

It is assumed that a wheel load, P , is applied uniformly upon a circular area having a radius, r . The vertical stress is distributed to a depth (thickness of base course), h , at a stress distribution angle, α . The vertical stress (pressure), p_i , at the interface between the base course and the subgrade can be estimated by means of the following equation (4):

$$p_i = \frac{P}{\pi(r + h \tan \alpha)^2} \tag{3}$$

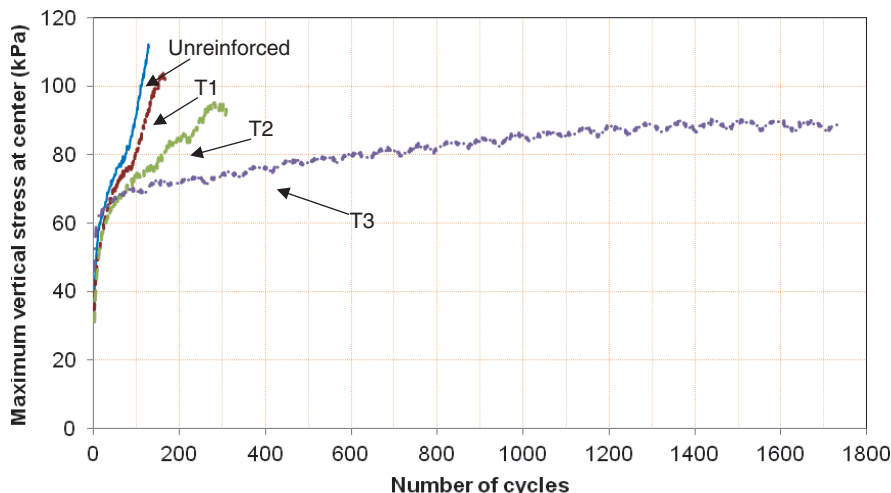


FIGURE 6 Maximum vertical stresses at interface between base and subgrade.

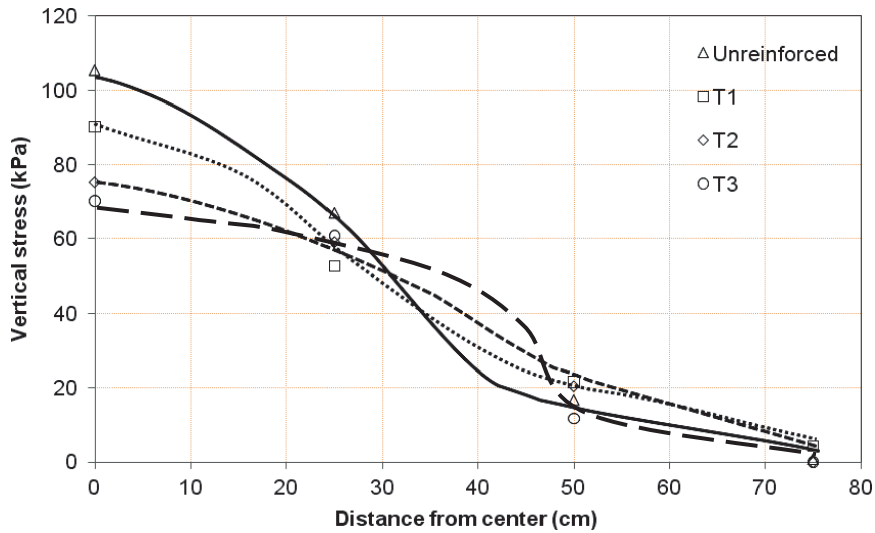


FIGURE 7 Vertical stress distributions at 120th load cycle.

From the measured maximum vertical stress at the interface, the applied wheel load, and the plate diameter, the stress distribution angle can be calculated for each cycle during the cyclic-loading test. Figure 8 shows the relationships between the reciprocal of the tangential values of the stress distribution angles and the number of load cycles. The initial values of $1/\tan(\alpha)$ for all the tests were close to 0.7 and increased nearly linearly on the logarithmic scale with an increase in the number of cycles. The deviation of the initial values of $1/\tan(\alpha)$ may be caused by the difference in the initial moduli of the base course and the subgrade, especially for the T3 geogrid-reinforced base, as discussed later. The contribution of the geogrid to the initial stress distribution angle is minimal because the base course is not fully engaged within the apertures of the geogrid at a small deformation. The unreinforced base course had a similar initial stress distribution angle as the geogrid-reinforced base courses. However, the stress distribution angles for the unreinforced base decreased with the number of cycles faster than those for the reinforced bases. In this case, the vertical stress for the unreinforced base course was concentrated near the center of the plate, which is consistent with the results discussed earlier in the stress analysis. In addition, the triangular-aperture

geogrids reduced the rate of reduction in the stress distribution angle, which led to a slow increase in the vertical stress at the center. The reciprocal of the tangential values of the stress distribution angles increased rapidly after the reciprocal reached approximately 1.2, which corresponds to 39.8° .

Modulus Analysis

The above discussion shows that, during the cyclic loading, the quality and integrity of the base course deteriorated, thus resulting in a reduction in the stress distribution angle. In all loading tests, cracks developed in the base courses around the loading plate during loading.

Some previous studies considered that the benefit of geosynthetic reinforcement is equivalent to increasing the thickness of the base course (15). In the current study, however, the benefit from the geosynthetic reinforcement is considered equivalent to increasing the modulus of the base course. Before Boussinesq’s solution is used, Odemark’s method (16) can be employed to transform a two-layer

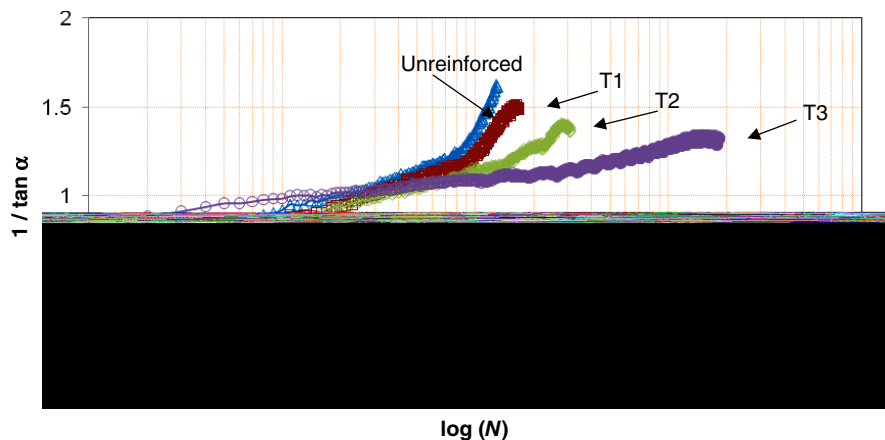


FIGURE 8 Relationship between stress distribution angle and number of cycles.

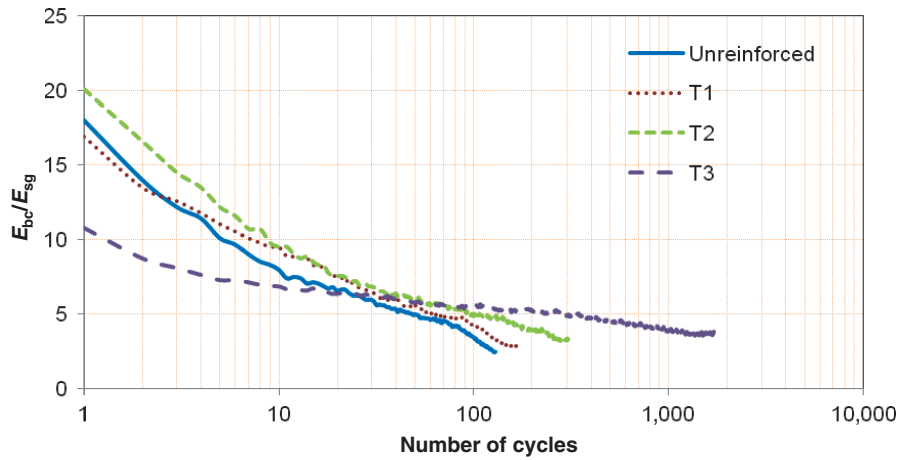


FIGURE 9 Modulus ratio of base course over subgrade versus number of cycles.

system (i.e., the base course and the subgrade) into an equivalent homogenous system. From the following formula, the equivalent thickness can be calculated:

$$h_e = h \left[\frac{E_{bc}(1 - \mu_2^2)}{E_{sg}(1 - \mu_1^2)} \right]^{\frac{1}{3}} \tag{4}$$

where

- h = thickness of base course (m),
- h_e = equivalent thickness (m),
- E_{bc} = elastic modulus of base course (MPa),
- E_{sg} = elastic modulus of subgrade (MPa),
- μ_1 = Poisson’s ratio of base course ($\mu_1 = 0.3$ chosen in this study), and
- μ_2 = Poisson’s ratio of subgrade ($\mu_2 = 0.5$ chosen in this study because subgrade was nearly saturated under cyclic loading, i.e., an undrained condition).

Qian et al. (17) obtained $E_{sg} = 29.4$ MPa from cyclic plate loading tests on the subgrade.

From the measured vertical stress at the center of the interface between the base course and the subgrade, the equivalent thickness of the base course can be calculated by using the following Boussinesq solution; then the modulus of the base course can be estimated from Equation 4 if the modulus of the subgrade is known:

$$\sigma_c = p \left[1 - \frac{h_e^3}{(r^2 + h_e^2)^{1.5}} \right] \tag{5}$$

where

- σ_c = vertical stress at center of interface between base course and subgrade (kPa),
- p = contact pressure on surface (kPa), and
- r = radius of equivalent tire contact area (m).

To use the equivalent thickness method, the following two requirements should be met: (a) the upper layer should have a higher modulus than the lower layer (with the recommendation that the modulus ratio of the upper layer to the lower layer be larger than 2) and (b) pref-

erence is for the equivalent thickness to be greater than the radius of the loading plate to make the method more accurate (16). The test conditions in this study met the preferred requirements for Odemark’s method. Figure 9 shows that the calculated modulus ratios for all test sections decreased with an increase in the number of cycles and approached 5.0 before having an accelerated reduction in the modulus ratio. This accelerated reduction may have resulted from the development of cracks in the base courses. Giroud and Han (4, 5) limited the maximum modulus ratio to 5.0 in their design method. Figure 9 shows that the T3 geogrid-reinforced section had a lower initial modulus ratio than other sections. This variation may result from the variability of the base course and the subgrade. As shown in Figure 7, the subgrade in the T3 geogrid-reinforced section had a slightly higher CBR value. Because the CBR value of the subgrade was low (approximately 2.0), a small deviation in the CBR value would have an obvious effect. This effect is reflected in the results of the TBR value, the initial stress distribution angle, and the initial modulus ratio for the T3 geogrid-reinforced base.

CONCLUSIONS

This paper presented an experimental study of unreinforced and triangular-aperture geogrid-reinforced bases over a weak subgrade under cyclic loading and a stress analysis based on the test results. The following conclusions can be drawn from this study:

1. Triangular-aperture geogrids improved the performance of the reinforced base courses over the weak subgrade compared with the unreinforced base. The average traffic benefit ratios for T1, T2, and T3 geogrids at 25-, 50-, and 75-mm permanent deformations were 1.4, 2.4, and 8.7, respectively. These traffic benefit ratios are experimental results and should not be used directly for design. A relationship between the field and laboratory performance is necessary to apply these ratios for design.
2. The measured maximum vertical stresses at the interface between the base and the subgrade increased with an increase in the number of load cycles because of the deterioration of the base course and reduction of the stress distribution angle.
3. Triangular-aperture geogrids significantly reduced the maximum vertical stress on the subgrade and resulted in a more-uniform stress distribution compared with the unreinforced base.

4. Triangular-aperture geogrids reduced the rate of reduction in the modulus ratio of the base course over the subgrade compared with the unreinforced section. As the test sections approached failure, the modulus ratio of the base course over the subgrade was approximately 5.0 for all test sections.

5. The more-robust, thicker, and higher-mechanical-property geogrid had more benefit in the improved performance of the reinforced base over the weak subgrade.

ACKNOWLEDGMENTS

This research project was sponsored by Tensar International. Joseph Cavanaugh, Nicholas Reck, and Mark Wayne of Tensar provided great help and technical guidance to this study. Howard Jim Weaver of the Department of Civil, Environmental, and Architectural Engineering (CEAE) at the University of Kansas (KU), designed, fabricated, and installed the loading system used for this study. Milad Jowkar of the CEAE Department at KU provided great assistance to the laboratory tests. All of this support is greatly appreciated.

REFERENCES

1. Das, B. M., and E. C. Shin. Strip Foundation on Geogrid-Reinforced Clay: Behavior Under Cyclic Loading. *Geotextiles and Geomembranes*, Vol. 13, No. 10, 1998, pp. 657–666.
2. Love, J. P. *Model Testing of Geogrids in Unpaved Roads*. PhD dissertation, University of Oxford, Oxford, United Kingdom, 1984.
3. Haas, R., J. Walls, and R. G. Carroll. Geogrid Reinforcement of Granular Bases in Flexible Pavements. In *Transportation Research Record 1188*, TRB, National Research Council, Washington, D.C., 1988, pp. 19–27.
4. Giroud, J. P., and J. Han. Design Method for Geogrid-Reinforced Unpaved Roads, I: Development of Design Method, *Journal of Geotechnical & Geoenvironmental Engineering*, Vol. 130, No. 8, 2004, pp. 775–786.
5. Giroud, J. P., and J. Han. Design Method for Geogrid-Reinforced Unpaved Roads, II: Calibration and Applications. *Journal of Geotechnical & Geoenvironmental Engineering*, Vol. 130, No. 8, 2004, pp. 787–797.
6. Dong, Y.-L., J. Han, and X.-H. Bai. A Numerical Study on Stress–Strain Responses of Biaxial Geogrids Under Tension at Different Directions. *Advances in Analysis, Modeling & Design: Proc., ASCE Geo-Institute GeoFlorida 2010*, Geotechnical Special Publication No. 199, West Palm Beach, Fla., Feb. 20–24, 2010, pp. 2551–2560.
7. Giroud, J. P. An Assessment of Geogrid Use in Trafficked Areas (or What Are the Challenges for the Future?). Presented at Jubilee Symposium on Polymer Geogrid Reinforcement, Institution of Civil Engineers, London, Sept. 8, 2009.
8. Dong, Y.-L., J. Han, and X.-H. Bai. Bearing Capacities of Geogrid-Reinforced Sand Bases Under Static Loading. *Ground Improvement and Geosynthetics, Proc., GeoShanghai International Conference*, Geotechnical Special Publication 207 (A. J. Puppala, J. Huang, J. Han, and L. R. Hoyos, eds.), Shanghai, China, June 3–5, 2010, pp. 275–281.
9. Dong, Y.-L., J. Han, and X.-H. Bai. Numerical Analysis of Tensile Behavior of Geogrids with Rectangular and Triangular Apertures. *Geotextiles and Geomembranes*, Vol. 29, No. 1, 2011, pp. 83–91.
10. Webster, S. L., R. W. Brown, and J. R. Porter. *Force Projection Site Evaluation Using the Electric Cone Penetrometer (ECP) and the Dynamic Cone Penetrometer (DCP)*. Technical Report GL-94-17. Waterways Experiment Station, U.S. Army Corps of Engineers, Vicksburg, Miss., 1994, 172 pp.
11. Qian, Y. *Experimental Study on Triangular Aperture Geogrid-Reinforced Bases over Weak Subgrade Under Cyclic Loading*. MS thesis, University of Kansas, Lawrence, 2009.
12. Gabr, M. *Cyclic Plate Loading Tests on Geogrid Reinforced Roads*. Research Report. North Carolina State University, Raleigh, 2001.
13. Lawton, E. C. Nongrouting Techniques. *Practical Foundation Engineering Handbook* (R. W. Brown, ed.), McGraw-Hill, New York, 1995, pp. 5.3–5.400.
14. Sigurdsson, O. *Geosynthetic Stabilization of Unpaved Roads on Soft Ground: A Field Evaluation*. MS thesis. University of British Columbia, Vancouver, Canada, 1991, 149 pp.
15. Giroud, J. P., and L. Noiray. Geotextile-Reinforced Unpaved Road Design. *Journal of Geotechnical Engineering*, Vol. 107, No. 9, 1981, pp. 1233–1254.
16. Ullidtz, P. *Pavement Analysis*. Elsevier Science Publishers, New York, 1987.
17. Qian, Y., J. Han, S. K. Pokharel, and R. L. Parsons. Determination of Resilient Modulus of Subgrade Using a Cyclic Plate Loading Test. In *Proc., GeoFrontier 2011*, ASCE Geo-Institute, Dallas, Texas, March 13–16, 2011.

The Committee for the 10th International Conference on Low-Volume Roads peer-reviewed this paper.